NMR Imaging of Multiphase Flow in Porous Media

Songhua Chen, Fangfang Qin, Kyung-Hoe Kim, and A. Ted Watson
Dept. of Chemical Engineering, Texas A&M University, College Station, TX 77843

Nuclear magnetic resonance (NMR) imaging techniques are used to determine porosity and saturation distributions. Difficulties in quantitation which arise from the short transverse relaxation times exhibited by fluids in porous media are addressed. Procedures are presented whereby transverse relaxation during the signal acquisition process is modeled to obtain accurate estimates of intrinsic magnetization intensity, and thus porosity and saturation. Special consideration is given to saturation/position dependence and multiexponential behavior of transverse relaxation. These procedures are validated with results for longitudinal profile images. The use of thin-slice cross-sectional profile images are demonstrated by observing fluid displacement in a rock sample with structural heterogeneities.

Introduction

Many petroleum reservoir processes involve the flow of two immiscible fluid phases (for example, oil and water) or three fluid phases (for example, oil, water, and gas). Porosity and fluid saturations are the basic quantitative measures for describing the amount of fluid phases present within local regions and are essential for describing the storage and transport of fluids in porous media. Conventional methods provide measures only as bulk or average properties. In contrast, NMR imaging techniques can provide unprecedented information about fluid phase distributions in porous media during displacement processes, as well as information about rock structures corresponding to local regions within porous media.

There have been a number of applications of NMR imaging to observe the distribution of fluids in porous media (Edelstein et al., 1988; Mandava et al., 1990; Osment et al., 1990; Chen et al., 1988; Baldwin and Yamanashi, 1986; Blackband et al., 1986; Chen et al., 1992). Most of these studies provide qualitative, or at best semiquantitative, measures of the amount of fluid phase observed at each location (or voxel). The main difficulty in quantitative evaluation of NMR images arises from the characteristically short transverse relaxation times associated with fluids in porous media. This feature is the result of the close proximity of fluid molecules to solid surfaces and is due to magnetic susceptibility and surface chemistry effects (Chen et al., 1992; Halperin et al., 1989; Glasel and Lee, 1979; Drain, 1962; Banavar and Schwartz, 1989). Therefore, significant relaxation may occur as the signals are acquired, with the result that the observed magnetization intensity may not be a good estimate of the intrinsic magnetization intensity. The intrinsic magnetization intensity is desired for evaluation of fluid saturations or porosity since it is proportional to the number of observed nuclei.

Accurate estimates of the intrinsic magnetization intensity, and thus the saturation and porosity, can be made if the effects due to transverse relaxation are accurately modeled and taken into account in analysis of the observed magnetization intensities. There are several difficulties associated with modeling transverse relaxation. Similarly to longitudinal relaxation (Halperin et al., 1989), transverse relaxation decay of fluids in porous media may not be modeled accurately using a single-exponential representation (Chen et al., 1992). Variations in rock pore structures and surfaces can lead to spatial variations in relaxation. Also, relaxation can vary with saturation (Chen et al., 1992; Watson et al., 1991). In this work, we present a method for quantitative evaluation of porosity and saturation distributions from NMR images that overcomes these problems.

Although the developed method can be applied to spin-density imaging with any number of spatial dimensions, we demonstrate it here with one-dimensional (profile) images. Due to the relatively short imaging time associated with acquiring profiles, these images are most useful for monitoring dynamic experiments. Two profile imaging sequences are demonstrated. Profiles which are obtained longitudinally along the direction of overall fluid displacement are useful for monitoring saturations in dynamic displacement experiments. This information can be of direct utility in modeling or estimating multiphase flow functions when the samples are relatively uniform throughout the cross section. For samples with laminated structures, useful information regarding fluid displacement can be

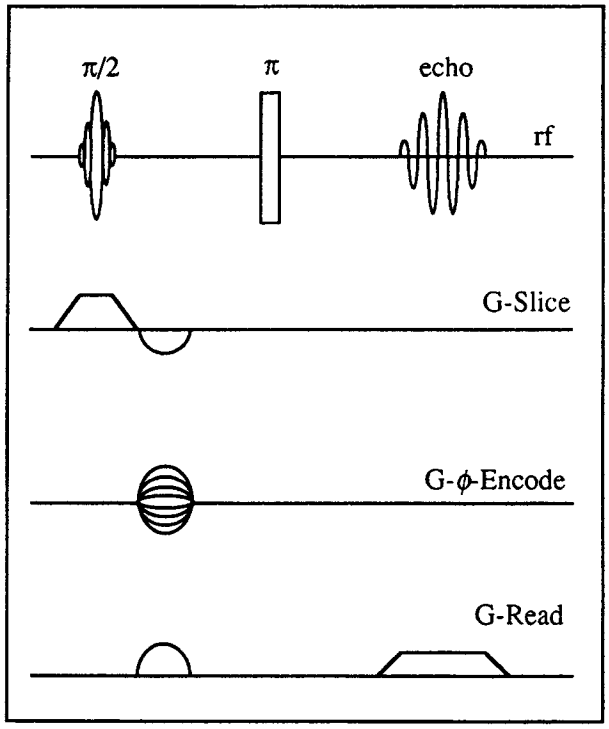

Figure 1. NMR imaging sequence.

obtained by acquiring multiple thin slices of cross-sectional profile images orthogonal to the direction of overall fluid flow.

Imaging Procedures

NMR imaging was performed with a GE 2-Tesla CSI-II System with a birdcage radio frequency (RF) coil. Cylindrically shaped rock samples were used in the displacement experiments and the superficial flow direction is along the axial direction of the cylinder. Two types of pulse sequences were used for acquiring profile images. These sequences are simplified versions of the two-dimensional imaging pulse sequence (Mansfield and Morris, 1982), which is illustrated in Figure 1. For acquiring multiecho longitudinal profiles, both the slice and phase encoding gradients are eliminated from the sequence shown in Figure 1, both the 90° and 180° pulses are hard (short duration, large amplitude) pulses, and the observation gradient is applied along the superficial flow direction. Routinely, we used 12–18 different *TE* values for a multiecho acquisition. For acquiring thin slice cross-sectional profiles, only the phase encoding gradient is eliminated. The phase of the 90° rf pulse determines the slice location of the imaged cross section and the slice gradient determines the slice thickness. The observation gradient is applied along the radial direction. Note that multiple slices can be obtained within a single delay time $TR \geq 5T_1$ using an automated slice-alternation technique, thus greatly reducing total imaging time, provided that slice-selective sinc pulses are used for both the 90° and 180° pulses and the spacing and thickness of slices are arranged such that no overlapping occurs between adjacent pulses.

The longitudinal (flow direction) profile imaging sequence is most useful for porous media with macroscopically homogeneous structures. For such systems, fluid storage is fairly uniform throughout cross sections perpendicular to the overall direction of fluid flow. Thus, those profiles can be used to observe the frontal displacement during dynamic experiments and to obtain the saturation distributions in both static and dynamic experiments. On the other hand, the thin slice cross-sectional profiles can be used to observe unstable displacements or displacements in sedimentary rocks that exhibit a laminated structure. The pore structure in such rocks may be quite uniform within bedding planes, but may vary appreciably across different bedding planes. The unique advantage of the multislice cross-sectional profile technique is that it highlights the variations among different bedding planes where appreciable variations are expected, while neglecting details within each plane, where the pore structure is relatively uniform. Also, the rapid multislice acquisition makes the sequence favorable for tracing fluid phases during displacements.

Theory

In the NMR profile imaging experiments, the spatial resolution is obtained by applying a magnetic field gradient G in one dimension. In this technique, the spatial information is represented in the frequency domain since

$$\omega = \gamma G z. \tag{1}$$

The image resolution is determined by the size of applied gradient G and is subject to the NMR linewidth of the sample under study (Mandava et al., 1990; Chen et al., 1992). Since fluids in porous media often exhibit broad NMR lines, a strong gradient may be required to achieve the desired spatial resolution. The use of NMR profile imaging techniques to detect fluid saturation is based on the fact that the intrinsic magnetization intensity $M_0(\omega)$ is proportional to the number of proton spins N within a pixel located along the z direction centered at the position determined by Eq. 1,

$$M_0(\omega) = k(z)N(z)\Delta z/\Delta\omega, \tag{2}$$

where

$$N(z) = \int\int_{A_{xy}} \rho(x,y,z)\,dx\,dy \tag{3}$$

is the proton linear density in the sample. For thin slice cross-sectional profiles with slice thickness Δz and spatial resolution in the x direction,

$$M_0(\omega) = k(x)N(x)\Delta x/\Delta\omega, \tag{4}$$

where

$$N(x) = \int_y\int_{\Delta z} \rho(x,y,z)\,dy\,dz, \tag{5}$$

is the proton density in a slab. For simplicity, longitudinal profiles will be used for the description of the general formalism in the remainder of this section. The same approach is applicable to the cross-sectional profiles as well.

The calibration constant $k(z)$ must be determined in order to obtain the linear density $N(z)$ from Eq. 2. The factor $k(z)$ depends on several experimental conditions, such as the amplifier receiver gain, the magnetic field strength and its homogeneity, the rf coil quality factor Q and the sample under study. Some of these quantities may change during the displacement experiments. Consequently, it is desirable to include a reference standard in the imaged volume in order to determine the proportionality factor at any time. If the reference is within the range where both rf and static field homogeneities are guaranteed, and any variation due to the sample is negligible, k can be treated as a constant and determined from

$$k=\frac{\int_{\Delta\omega_r} M_0^r(\omega)d\omega}{\int_{\Delta z_r} N^r(z)dz}. \tag{6}$$

The fluid phase saturation distribution can be calculated by

$$S(z)=N(z)/N_i(z), \tag{7}$$

where $N_i(z)$ is the linear proton density measured when the sample is fully saturated (such as prior to displacement). The porosity distribution $\phi(z)$ can be determined by

$$\phi(z)=N_i(z)/(\varrho A_{xy}), \tag{8}$$

where ϱ is the proton density of the observed fluid phase.

The main difficulty in quantitation arises from the fact that the acquired profile intensity measured at finite echo times TE is not the intrinsic magnetization $M_0(\omega)$ due to relaxation effects. If the relaxation processes were suitably represented by parameters T_1 and T_2, and the parameters were uniform throughout the medium, the relation between the observed and intrinsic magnetization intensities could be expressed as follows (Mandava et al., 1990):

$$M(\omega,TE,TR)=M_0(\omega)f(T_1,TR)g(T_2,TE). \tag{9}$$

Knowledge of the relaxation functions and parameters would allow for estimation of the intrinsic intensity from the observed intensity.

The effects of T_1 relaxation can be readily eliminated if sufficiently long delay time TR is used since the function $f(T_1,TR)$ approaches unity when $TR>5T_1$. This condition was adhered to all our experiments. On the other hand, the effects of T_2 can be eliminated only if the echo time TE were much less than T_2, a condition typically not observed for fluids in porous media. For porous rocks, values of T_2 are of the order of milliseconds and equipment limitations do not allow T_2 effects to be eliminated.

Previously, a simple approach was reported (Mandava et al., 1990) in which T_2 relaxation was assumed to be uniform throughout the sample and was represented by a single exponential model using a single, average value of T_2 corresponding to that measured at the fully saturated state. Using this approach, the transverse relaxation function in Eq. 9 is

$$g(T_2,TE)=\exp(-TE/T_2). \tag{10}$$

This function was used to represent both the sample and reference in the previous study.

Since the transverse relaxation depends on the sizes of pores in which the fluid resides, as well as on local surface composition, a single, averaged value may not accurately represent relaxation behavior in porous media which has a distribution of characteristic pore sizes. In addition, the distribution of pore sizes occupied by the observed fluid phase will change as saturation changes, resulting in the observed relaxation rate being a function of saturation.

We have developed a new approach in which the effects of spatial variation and saturation dependence of transverse relaxation, as well as nonsingle-exponential relaxation behavior, can be largely taken into account for determining porosity and saturation. The method involves the acquisition of profile images for several different values of TE and the determination of intrinsic intensity of magnetization by extrapolation of echo amplitudes to zero echo time ($TE=0$) in a model of intensity evolution. Since in this approach relaxation parameters are determined on a pixel-by-pixel basis for each saturation state observed, better estimates for the intrinsic magnetization intensity are obtained.

A multiexponential representation has been used successfully to represent longitudinal and transverse relaxation of fluids in porous media (Schmidt et al., 1986). This corresponds to the representation of porous media as a discrete set of collections of pores, each with a characteristic relaxation time. With a sufficient number of components, this model should adequately represent the relaxation process in a wide variety of rock samples.

Using the multiexponential representation, the observed intensity of magnetization corresponding to the ith pixel can be represented by

$$M(\omega_i,TE)=\sum_{j=1}^{N_C} M_{0j}(\omega_i)\exp(-TE/T_{2ij}). \tag{11}$$

Note that this representation allows for the use of different relaxation parameters at different positions. Estimates for the intensities and relaxation parameters are obtained by nonlinear regression through minimization of the following performance index for the ith pixel:

$$J_i=\sum_{l=1}^{n}[M^{\text{obs}}(\omega_i,TE_l)-M^{\text{cal}}(\omega_i,TE_l)]^2, \tag{12}$$

where the calculated values M^{cal} are provided by the representations in Eq. 11. Estimates are obtained for $[M_{0j}(\omega_i),T_{2ij}]$, $j=1,\ \ldots,\ N_c$, for each pixel. The intrinsic intensity of magnetization for the ith pixel is the sum:

$$M_0(\omega_i)=\sum_{j=1}^{N_c} M_{0j}(\omega_i). \tag{13}$$

A useful criterion for selection of the appropriate number of terms for the multiexponential model is the F-test (Beck and Arnold, 1977; Draper and Smith, 1981). One can test whether a more complete model is warranted by comparing a tabulated value with a statistic calculated using values of the residual sum of squares (RSS) obtained using the more complete model (with N_c components) with the simpler model (with

$N_c - 1$ components). The calculated statistic is

$$F = \frac{[RSS(N_c - 1) - RSS(N_c)]/p}{RSS(N_c)/(n - m)}, \tag{14}$$

where n = number of observed data, $m = 2N_c$ and $p = 2$ is the difference between the number of components in the simpler and more complete models. If the tabulated value exceeds the calculated value, one concludes (at the specified level of significance) that the available data do not warrant inclusion of the additional terms in the more complete model. For nonlinear regression, the confidence level is said to be approximate (Beck and Arnold, 1977).

The actual number of components identified will in general depend on the number of echo times and the accuracy of the measurements. The objective here is not precise resolution of the components, but rather good estimates for the intrinsic magnetization. It should be noted that any components that have undergone complete relaxation before the first echo time will not be observed. The minimum echo time is limited by the equipment. If a significant fraction of the fluid has such small relaxation times, which may occur in certain microporous materials, the intrinsic intensity will not be accurately estimated.

An alternative model for representations of relaxation is provided by the stretched exponential relaxation model (Kenyon et al., 1988)

$$M(\omega_i, TE) = M_0(\omega_i)\exp[-(TE/T_{2i})^{\alpha_i}]. \tag{15}$$

The stretched exponential was shown to arise from a distribution of single exponential relaxation times weighted towards short times (Kenyon et al., 1988). They showed that a stretched exponent α of 0.67 results from a half-Gaussian distribution of relaxation times. This model has been used to represent longitudinal relaxation of water in sandstone samples. When this is a suitable representation, it is more convenient than the multiexponential model since relatively fewer parameters are required. Estimates of the parameters $M_0(\omega_i)$, T_{2i}, and α_i can be obtained by nonlinear regression using Eqs. 12 and 15.

Various simplified situations may also be of interest. For example, one could assume that the relaxation parameters in the previous models are uniform throughout the sample. This analysis is useful for evaluating different relaxation models by comparing results for average values obtained from NMR measurements with those by gravimetric methods. It is expected that this treatment would be valid for determination of porosity in relatively uniform samples, but would likely not be suitable for samples with distributions of saturations as commonly occurs during multiphase flow processes. This simplified procedure will be demonstrated in the Results and Discussion section.

Experimental Details

Static and dynamic displacement experiments have been conducted using several different types of rock samples, including Indiana, Texas Cream and building block limestones, as well as Berea, Bentheimer and Brown (Massiallon) sandstones. All samples are prepared in cylindrical shape with 2.54 cm diameter but in different lengths. For those samples used only for static experiments, distilled water was used to saturate the core samples and a shrinkable Teflon tube was used for wrapping the core samples to prevent evaporation during NMR measurements. The samples used for displacement experiments were mounted in plexiglass core holders and sealed using an epoxy (Stycast 2651) sealant. The epoxy has much shorter T_2 and T_2^* values than the fluids saturating the porous rocks so that it does not contribute to the signal intensity. Deuterium oxide (D_2O) was used as the aqueous phase, and either *n*-octadecene or *n*-hexadecane was used as the oleic phase. Protons are imaged so that only the oil phase is observed. In these displacement experiments, each core sample was first saturated with the oleic phase and the aqueous fluid phase was injected at one end until no further displacement of the oleic phase was observed. Most of our displacement experiments were primary imbibitions except for the Brown sandstone sample, in which case both primary imbibition and drainage processes were carried out. The pressure drop across the sample was recorded during the displacements. A reference standard of gel solution consisting of agarose powder and 0.005-M $CuSO_4$ solution was prepared and taped to the sample holder as a reference standard for signal intensity calibration.

Results and Discussion

Quantitative evaluation of saturation and porosity

The role of model selection in making quantitative estimates is demonstrated using data obtained with samples that are fully saturated with a single fluid phase. An Indiana limestone sample was saturated with oil and two building limestone samples were saturated with distilled water. The selected samples appeared to be relatively uniform and estimated relaxation parameters did not exhibit significant variation with position. In order to validate the quantitative estimates, we compared estimates of the average porosity with those values determined gravimetrically. First, the average values were computed using the simplified procedure in which the regression analysis was performed with the integrated signal. Using this method, possible variation of transverse relaxation with position is ignored. However, this assumption was checked by calculating relaxation parameters for selected models on a pixel-by-pixel basis, as outlined in the Theory section and comparing the average of the profile with the previously calculated averages and gravimetric values. This latter approach does not require any assumptions regarding the spatial uniformity of transverse relaxation.

Regression results for the Indiana limestone samples are summarized in Table 1. A substantial reduction in the residual sum of squares was obtained when using a biexponential representation as compared to a single exponential. Little further reduction was obtained using a triexponential representation.

Table 1. Regression Results for Building Limestone

N_c	RSS (Scaled*)	R^2	F value**	$F_{0.95}$ $(q, n-m)$
1	90.8	0.990		
2	1.29	1.000	450	3.81
3	1	1.000	1.8	3.89

* Scaled to unity for triexponential model ($N_c = 3$).
** Calculated with present and previous model.

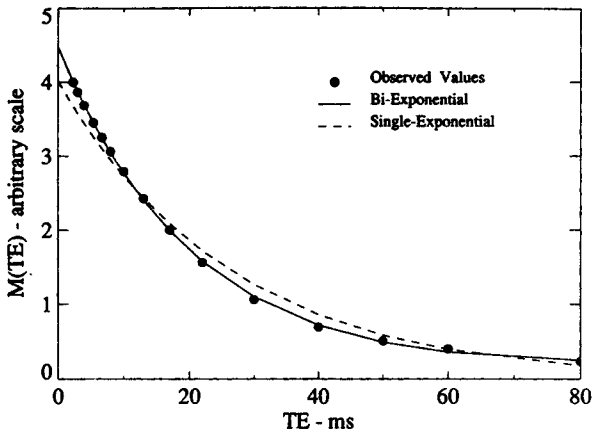

Figure 2. Measured intensities with estimates for single- and biexponential models (Indiana limestone sample).

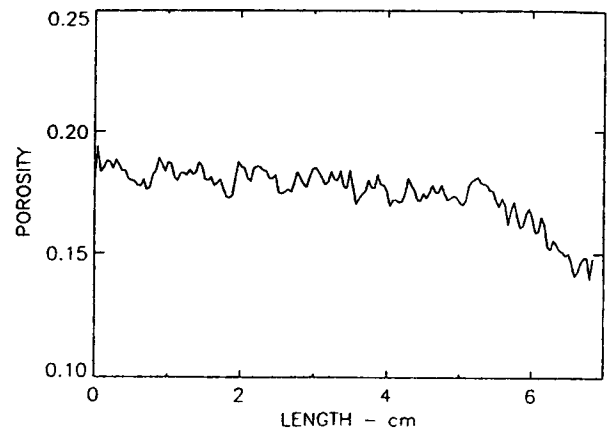

Figure 3. Porosity profile for Indiana limestone sample.

The selection of the biexponential model is supported by the F-test (see Table 1). The measured values of $M_0(\omega)$ are plotted with the calculated values determined with the single- and biexponential models in Figure 2. The latter model provides a much more precise fit of the data. The value estimated for the average porosity was 17.7%, which is within 5% of the value obtained gravimetrically (which was 16.9%). Neither the single exponential nor the stretched exponential provided accurate estimates. Errors in estimates obtained with those models were 19% and 13%, respectively.

The calculated porosity distribution is shown in Figure 3. In these calculations, the model selection procedure to determine the appropriate number of components was first carried out for several selected pixels. Since for each case the biexponential model was chosen, that model was then used for each of the pixels. The readout gradient $G = 3.25$ Gauss/cm (1,350 Hz/mm for protons) was used in the experiment. The pixel size of 0.42 mm corresponds to the resolutions of this experiment since the frequency resolution of $\Delta\nu = 567$ Hz/pixel is much larger than the overall NMR linewidth for this sample, which is approximately 200 Hz. The porosity distribution appears roughly uniform throughout much of the sample, although it does decrease in the righthand portion of the sample. The degree to which the pixel-to-pixel variation reflects actual variation in the local porosity values is a little difficult to assess. An estimate of the noise level can be obtained by analyzing a region in the profile which does not include the sample. The ratio between the standard deviations calculated in such a void region with that of a similarly sized region corresponding to a relatively uniform portion of the sample is approximately 1:8, indicating that much of the signal variation may well be due to variations in the local porosity. A more accurate assessment could be made through analysis of replicate experiments. It is noted that the accuracy can be improved through additional signal averaging. The average value for the porosity distribution is 17.5%, which compares well with the value calculated with the integrated signal and the gravimetric analysis (see Table 2).

Similar analyses were conducted with three other samples, including two different building limestones and a Texas Cream limestone. For these samples, the biexponential model was again chosen by the model selection procedure. Average porosity values for these samples calculated using the biexponential model were within a few percent of those obtained gravimetrically, while estimates using the single- and stretched-exponential models yielded noticeably larger errors (see Table 2).

The importance of considering saturation dependence of transverse relaxation for determination of saturation distributions is demonstrated next. A Bentheimer sandstone sample was initially saturated with distilled water, then desaturated with pressurized N_2. The process was stopped before reaching an equilibrium saturation state. Longitudinal multiecho profiles were acquired using 17 different values of TE. Figure 4 shows the saturation profile calculated from the multiecho intensity profiles using Eqs. 10 and 12 with $N_c = 1$ (single-exponential model). We see that the fluid distribution is nonuniform. A plot of T_2 as a function of saturation was prepared by matching the T_2 value for each pixel with the respective value of saturation. Figure 5 shows a significant variation in T_2 with saturation. This variation is taken into account in our

Table 2. Porosity Estimation Using Different Relaxation Models

Samples	Porosity (% Error)				
	Gravimetric Method	Integrated Signal			Avg. Distrib. (Bi-Exp.)*
		S-Exp.	Bi-Exp.	Stretch-Exp.	
Indiana Limestone	16.9	20.1(19%)	17.7(5%)*	19.1(13%)	17.5(3%)
Building Limestone A	18.9	21.4(13%)	19.1(1%)*	21.5(14%)	19.4(3%)
Building Limestone B	19.2	21.1(10%)	19.1(−1%)*	21.0(9%)	19.2(0%)
Texas Cream Limestone	24.2	25.5(5%)	25.0(3%)*	25.1(4%)	24.9(3%)

* Selected model

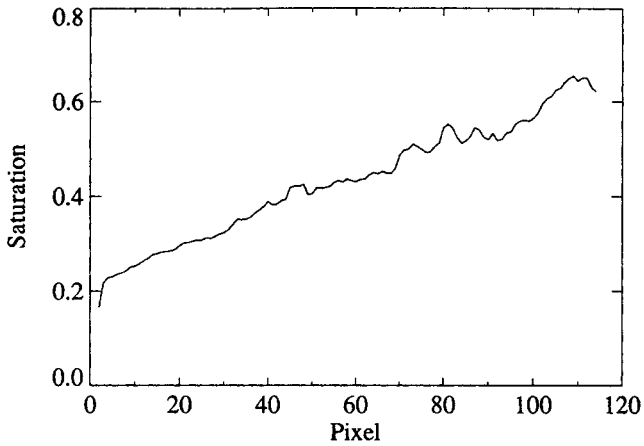

Figure 4. Saturation profile in Bentheimer sandstone sample.

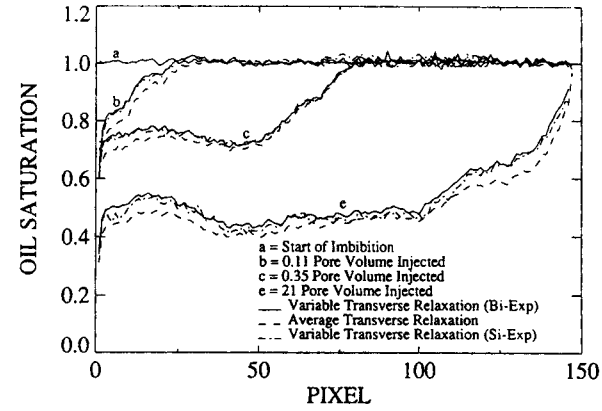

Figure 6. Saturation profiles for different models for building limestone sample.

analysis by estimating relaxation parameters on a pixel-by-pixel basis. It is interesting that the T_2 values for the fully saturated sample did not vary significantly across the sample (the overall value was 16 ms).

Some results obtained during a dynamic displacement are presented next. A relatively uniform building limestone sample was initially saturated with *n*-octadecene, and D_2O was injected from one end at a rate of 2 mL/h. Longitudinal proton intensity profiles were acquired at various times. At each of the times, several profiles with different echo times ranging from 2.5 ms to 50 ms were taken so that the intrinsic intensity of magnetization and relaxation parameters could be estimated on a pixel-by-pixel basis. The imaging time for each profile is given by the product of the repetition time (or time between consecutive pulse sequences), the number of echo times and the number of acquisitions for each echo time. For these experiments, the delay time was 2.1 s, approximately 15 different echo times were used, and there were four acquisitions for each echo. Thus, the total imaging time for each profile was approximately two min. The linear displacement during this time is submillimeter, but it is not so small as to guarantee no saturation changes during that time (Mandava et al., 1990).

Results are presented for the initial state and saturation states obtained after injection of 0.11, 0.35 and 21 pore volumes.

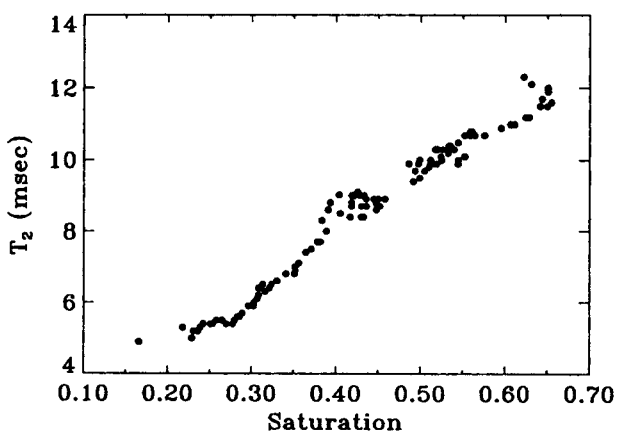

Figure 5. Saturation dependence of T_2 for Bentheimer sandstone sample.

Examination of several pixels indicated that the biexponential model appeared to be the most appropriate among the multiexponential models. Saturation values calculated with these models are shown in Figure 6 with values calculated by two other methods. In one of the methods, the relaxation parameters were also calculated on a pixel-by-pixel basis, but with a single-exponential model. In the other method, only a single, average value of T_2 for the sample measured at complete saturation was used for determining the intrinsic intensity for each saturation state. The variation of T_2 with saturation is not taken into account by the latter method.

Since there is little difference among the profiles for the initial saturation state, it appears that T_2 variation under conditions of complete saturation is also negligible for this sample. However, it is observed that the saturation profiles calculated at low saturations using the different approaches show considerable departures due to variations in transverse relaxation with saturation. Generally speaking, if the T_2 value corresponding to the initial saturation is used for all cases, the calculated saturation at partial saturations will be smaller than the true value since T_2 values decrease with saturation. Note that failure to account for relaxation variations with saturation would result in substantial material balance errors for this sample. In this sample, the average value of T_2, using a single-exponential model, was 13.9 ms at full saturation and decreased to 9 ms after 21 pore volume of D_2O was injected. Some differences are also seen between the cases in which different relaxation models were used.

Observing displacements in laminated structures

The use of thin-slice cross-sectional profiles to observe fluid displacement in rocks with structural heterogeneities is demonstrated in this section. NMR measurements were performed on a Brown (Massiallon) sandstone sample. This sample has laminated structures with bedding planes that exhibit a small angle with respect to the axial direction. Within each thin slice, the bedding planes are nearly perpendicular to the superficial flow direction. The resolved spatial dimension is selected to be perpendicular to the bedding planes in each thin-slice cross section, as illustrated in Figure 7. This arrangement results in signal integration across the various bedding planes, where the saturation is expected to be fairly uniform. The images can be

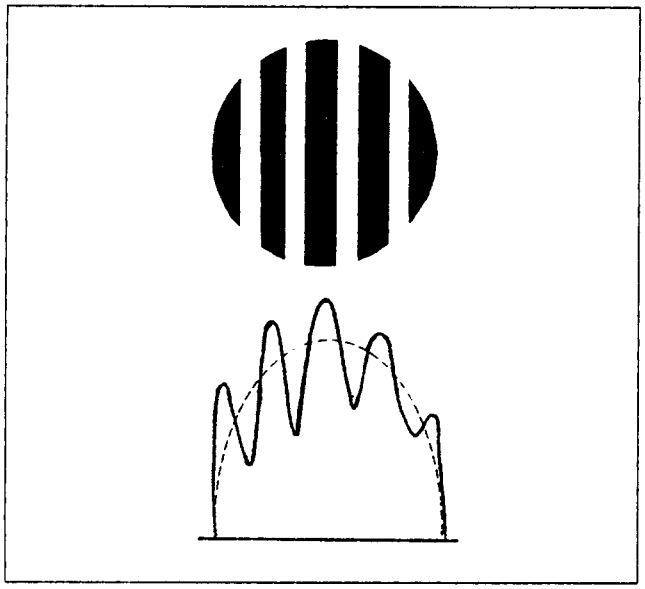

Figure 7. Cross-sectional profile orientation.

used to observe the relative rates of fluid displacement among the various bedding planes.

Profile images were acquired during two-phase displacement experiments consisting of primary imbibition and drainage processes. The wetting phase was D_2O and the nonwetting phase was hexadecane. A series of six different flow rates, listed in Table 3, were used for both the imbibition and drainage cycles. The lowest one (2 mL/h) is equivalent to a superficial velocity of 0.45 m/d, which is typical of reservoir fluid flow. Each flow rate was maintained sufficiently long until essentially no more of the displaced fluid was produced. Thus, a sequence of "steady states" was attained in the dynamic displacement experiments. Pressure drops across the rock sample were measured during the displacements; the pressure drop values for the respective flow rates are also listed in Table 3.

For multiple thin-slice transverse cross-sectional profile images, quantitative determination of saturations from the observed intensities can be obtained using either of the following two methods. In the first method, a long uniform reference standard may be taped along the length of the core. Thus on each slice of the transverse cross-sectional profile, the reference signal will be on the side of the image, and the identical procedures to that used for longitudinal profiles can be used for quantitative comparison. One drawback of this approach is that the longitudinal profiles cannot be easily obtained. Another method which does not have this disadvantage can be used for obtaining quantitative results. First, the saturation profiles along the axial direction are determined using longitudinal profiles, as described in the previous section. Second,

Table 3. Flow Rate and Steady-State Pressure-Drop Values

q (mL/h)	2	4	7.5	15	40	100
Imbibition ΔP(Pa)				15,900	29,600	49,000
Drainage ΔP(Pa)		6,900	7,580	8,270	15,200	29,000

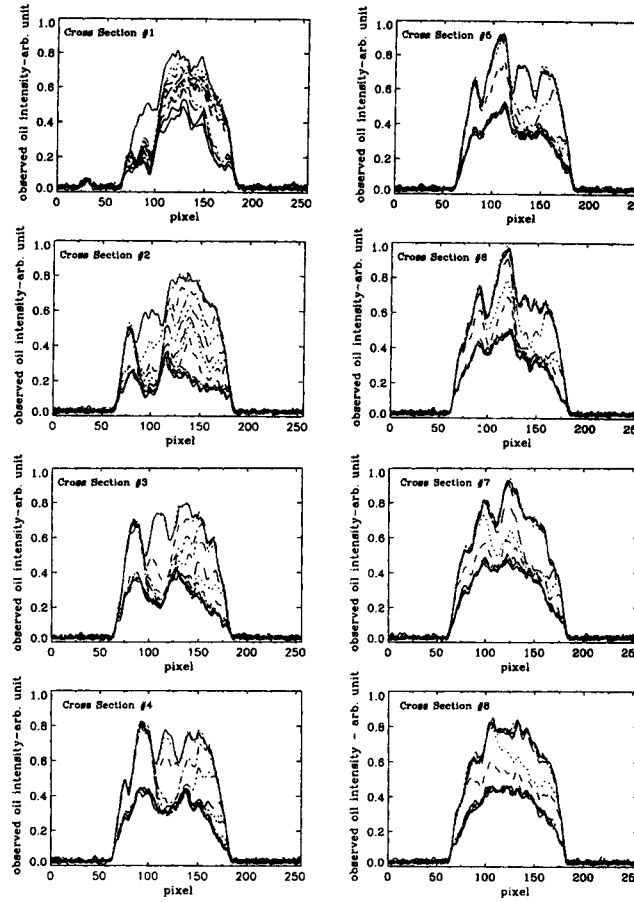

Figure 8. Oil displacement during imbibition experiment in a laminated Brown sandstone sample.

integrated signals of individual thin-slice transverse cross-sectional profiles are determined using multiecho cross-sectional profile data for each slice. The integrated signal of each slice is then scaled to the signal from the corresponding pixels on the longitudinal saturation profile and from which average saturation corresponding to individual slice profiles were determined. Once this average value is obtained, the saturation variation within a cross-sectional profile can be determined. For the purpose of the present study, a semiquantitative description based on single-echo time acquisitions will be presented.

Figure 8 shows plots of the observed magnetization intensity of oil for eight slices, each showing 13 profiles taken during the first stage of imbibition ($q = 2$ mL/h). Each slice is $\Delta z = 4$ mm in thickness and slice spacing is 7.5 mm. In the experiments, the readout gradient $G = 7.21$ Gauss/cm (3,000 Hz/mm for proton) was applied along the x direction, which is perpendicular to the flow direction z. This gradient results in a profile resolution of 0.186 mm/pixel. This resolution is much higher than the typical layer thickness in the Brown sandstone, which is of the order of one to a few millimeters. Thus, the laminations can be well identified. Since the frequency resolution per pixel is 558 Hz using this gradient, and the linewidth of the water-saturated Brown sandstone is 570 Hz, there may be some signal overlap between adjacent pixels (Mandava et

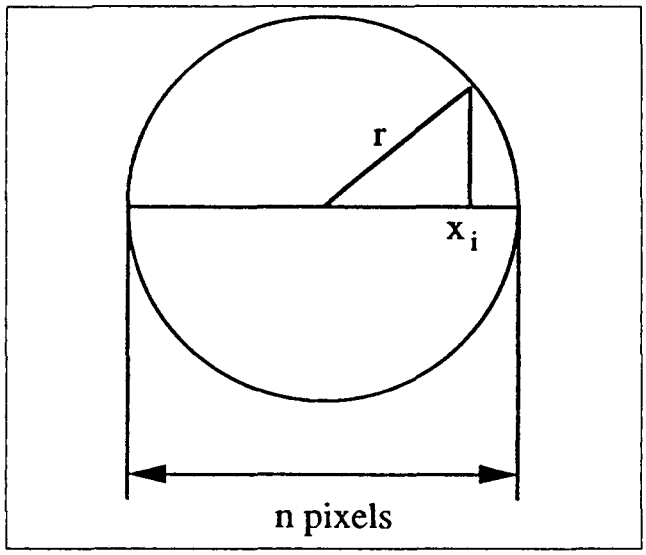

Figure 9. Intensity scaling.

al., 1990). This does not affect our ability to distinguish the bedding planes, which are an order of magnitude larger than the pixel size. In this experiment, eight repetition acquisitions were performed for each slice profile for improving signal-noise ratio. The total imaging time of the eight acquisitions for obtaining each slice profile is 16 s. In these plots, No. 1 slice was next to the inlet, and No. 8 was closest to the outlet. The 13 profiles correspond to approximate displacement times $t=0$, 7, 15, 23, 32, 44, 53, 65, 102, 120, 135, 163 and 192 min. after the start of water injection. A digital filtering process was applied to the raw data to reduce certain random noise only for the purpose of displaying the profiles. Since the bedding planes are at an angle with respect to the axial direction, the various laminations appear at different positions in different slices. Note, for example, how the lamination which appears at the left of cross section No. 3 is near the center in the cross section No. 7 (the two slices are 30 mm apart). The initial (fully saturated) state corresponds to the highest intensity profiles on those plots.

During imbibition, the oil saturation decreases as it is displaced with D_2O, which is demonstrated in the figure as the reduction in the oil profile intensities. These profiles indicate that fluid is displaced in the various layers at different rates. For example, note how displacement in the layer on the left in cross-section No. 3 takes place only after it has taken place through the rest of the slice. This nonuniformity in displacement profiles can be explained by permeability variations among different laminations.

Since we used samples with circular cross sections, the observed intensity profiles in Figure 8 correspond to the hypotenuse-weighted intensities; that is, the intensities of each pixel do not represent the same size sample volume. For obtaining unit volume intensities of each pixel, the following geometrical scaling can be used:

$$M_{\square}(i) = M_{\bigcirc}(i) \Big/ \left\{ 2 \sin \left[\arccos \frac{x_i}{n_p/2} \right] \right\}, \qquad (16)$$

where x_i is the pixel location, as illustrated in Figure 9. The

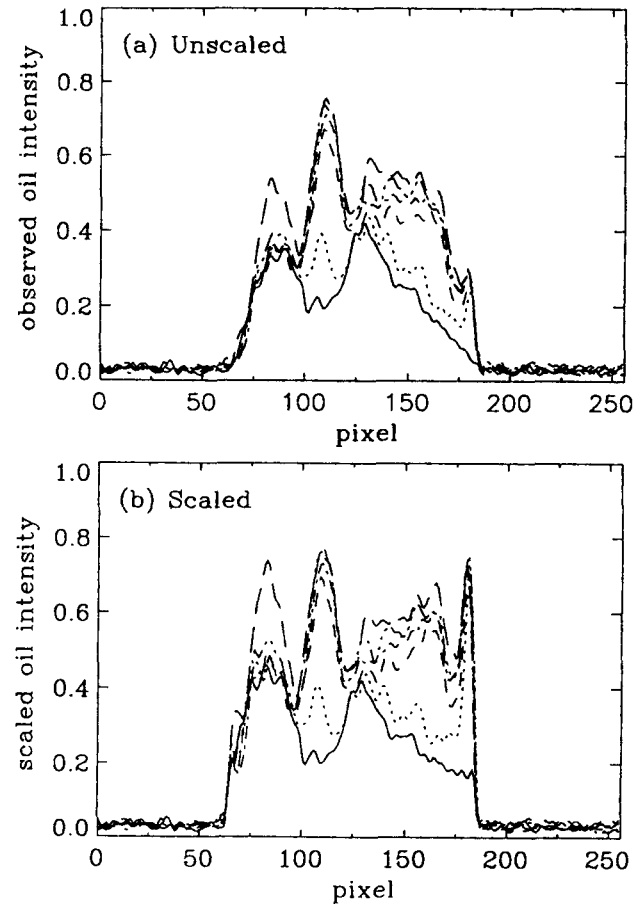

Figure 10. Unscaled vs. scaled intensity profiles.

quantity $M_{\square}(i)$ is the unit volume intensity, and $M_{\bigcirc}(i)$ is the observed intensity.

Using this scaling, we can obtain the difference of unit volume fluid saturations in individual bedding planes. A comparison between the scaled and unscaled profiles in one slice, corresponding to fluid saturation changes during the first hour after the start of the drainage process, is shown in Figure 10. Significant variations in porosity and permeability among the various laminations are apparent. Eight different regions corresponding to laminations can be identified in the figure. Note that the displacement occurred most rapidly in the third and eighth regions, and slowly in the first, second, fourth and fifth regions.

The variations of fluid wetting characteristics (Dullien, 1979; Anderson, 1986a,b) in different laminations can be visualized by observing different steady-state profiles. Figure 11 shows intensity profiles for a single circular cross section corresponding to each of the steady states obtained using the injection rates listed in Table 3. We see that essentially all the mobile oil was displaced during the first stage of water injection ($q=$ 2 mL/h); increasing the flow rate does not result in further displacement of oil. In contrast, the drainage profiles show that oil saturation continued to increase as the flow rate was increased. Observation of sequential steady states indicate that the sample is water wet and that the relative wetting does not vary significantly among the layers. It appears that the struc-

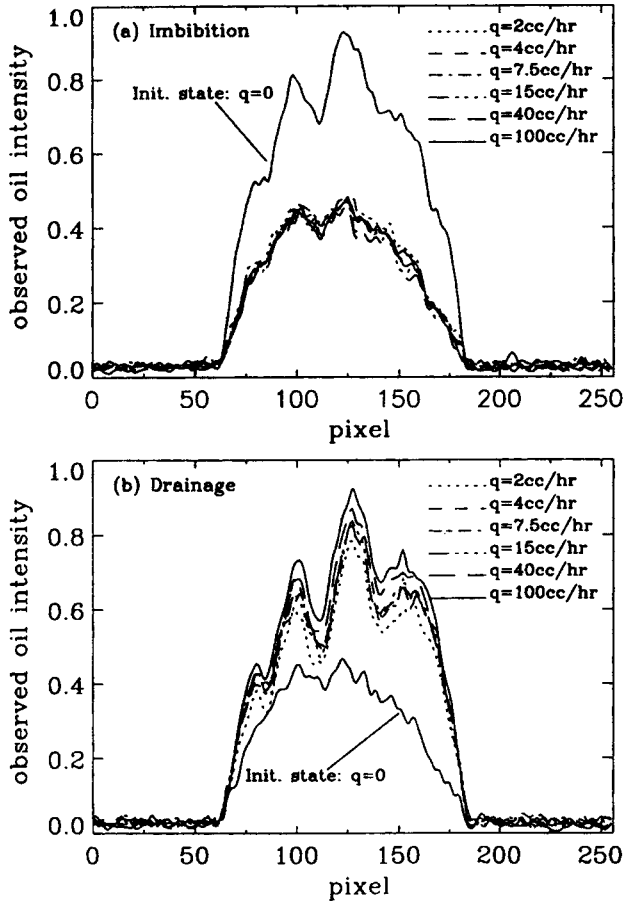

Figure 11. Flow rate dependence of saturations in (a) imbibition and (b) drainage experiments in the Brown sandstone sample.

tural heterogeneity of the rock sample does not result in significant heterogeneity of fluid wetting characteristics.

Conclusions

Procedures have been developed whereby porosity and fluid saturation distributions in porous media can be determined accurately from NMR images. The procedures are based on modeling transverse relaxation during the image acquisition process. We found that accurate quantitation requires consideration of spatial variations and saturation dependence of transverse relaxation, as well as selection of an appropriate model for representation of transverse relaxation. The biexponential representation was most appropriate for the limestone samples we studied. Thin-slice cross-sectional profiles were used to observe flow in a sandstone sample that exhibited a laminated structure.

Acknowledgment

This project was supported by DOE Grant #DE-FG07-89BC14446. Financial assistance was also obtained from a University-Industry Cooperative Program at Texas A&M University and from the Center for Energy and Mineral Resources. The authors would like to thank Mr. Hsie-Keng Liaw who prepared the Bentheimer sandstone sample for one of the experiments.

Notation

f = function for T_1 effect
g = function for T_2 effect
J = performance index
k = calibration constant
M = intensity of magnetization
M_0 = intrinsic intensity of magnetization
M_0^r = M_0 corresponding to reference standard
M^{cal} = calculated M
M^{obs} = observed M
n_p = number of pixels
N = linear proton density
N_c = number of components
N_i = linear density corresponding to $S=1$
N^r = linear density corresponding to the reference
p = difference between number of parameters in models
q = flow rate
RSS = residual sum of squares
$RSS(N_c)$ = RSS using model with N_c components
S = fluid saturation
TE = echo time
TR = NMR pulse sequence repetition time
T_1 = longitudinal relaxation time
T_2 = transverse relaxation time
T_2^* = characteristic time for echo envelope

Greek letters

α = stretched exponent
γ = proton gyromagnetic ratio
ρ = proton density in porous media
ϱ = proton density in fluid
ϕ = porosity
ω = angular frequency
$\Delta\omega_r$ = ω domain width across reference standard
Δz_r = length across reference standard

Literature Cited

Anderson, W. G., "Wettability Literature Survey—Part 1: Rock/Oil/Brine Interactions and the Effects of Core Handling on Wettability," *J. Pet. Tech.*, **38**(11), 1125 (1986).

Anderson, W. G., "Wettability Literature Survey—Part 2: Wettability Measurements," *J. Pet. Tech.*, **38**(12), 1246 (1986).

Baldwin, B. A., and W. S. Yamanashi, "Detecting Fluid Movement and Isolation in Reservoir Cores Using Medical NMR Imaging Techniques," *Soc. Petroleum Eng. Annual Tech. Conf.*, SPE paper #14884, p. 39 (1986).

Banavar, J. R., and L. M. Schwartz, "Probing Porous Media with Nuclear Magnetic Resonance," in: *Molecular Dynamics in Restricted Geometries*, J. Klafter and J. M. Drake, eds., John Wiley & Sons, New York, pp. 273-310 (1989).

Beck, J. V., and K. J. Arnold, *Parameter Estimation in Engineering and Science*, Wiley, New York (1977).

Blackband, S., P. Mansfield, J. R. Barnes, A. D. H. Clague, and S. A. Rice, "Discrimination of Crude Oil and Water in Sand and in Bore Cores with NMR Imaging," *SPE Form. Eval.*, **1**, 31 (1986).

Chen, J., M. M. Dias, S. Patz, and L. M. Schwartz, "Magnetic Resonance Imaging of Immiscible Fluid Displacement in Porous Media," *Phys. Rev. Lett.*, **61**(13), 1489 (1988).

Chen, S., K.-H. Kim, F. Qin, and A. T. Watson, "Quantitative NMR Imaging of Multiphase Flow in Porous Media," *Mag. Reson. Imag.*, **10**, 815 (1992).

Drain, L. E., "The Broadening of Magnetic Resonance Lines due to Field Inhomogeneities in Powdered Samples," *Proc. Phys. Soc.*, **80**, 1380 (1962).

Draper, N. R., and H. Smith, *Applied Regression Analysis*, 2nd ed., John Wiley & Sons, New York (1981).

Dullien, F. A. L., *Porous Media, Fluid Transport and Pore Structure*, Academic Press, New York (1979).

Edelstein, W. A., H. J. Vinegar, P. N. Tutunjian, P. B. Roemer, and O. M. Mueller, "NMR Imaging for Core Analysis," *Soc. Petroleum Eng. Annual Tech. Conf.*, SPE paper #18272, Houston (Oct. 2-5, 1988).

Gallegos, D. P., and D. M. Smith, "A NMR Technique for the Analysis of Pore Structure: Determination of Continuous Pore Size Distribution," *J. Colloid Inter. Sci.*, **122**(1), 143 (1988).

Glasel, J. A., and K. H. Lee, "On the Interpretation of Water Nuclear Magnetic Resonance Relaxation Times in Heterogeneous Systems," *J. Am. Chem. Soc.*, **96**, 970 (1979).

Halperin, W. P., F. D'Orazio, S. Bhattacharja, and J. C. Tarczon, "Magnetic Resonance Relaxation Analyses of Porous Media," in: *Molecular Dynamics in Restricted Geometries*, J. Klafter and J. M. Drake, eds., John Wiley & Sons, New York, pp. 311-350 (1989).

Kenyon, W. E., P. I. Day, C. Straley, and J. F. Willemsen, "A Three-Part Study of NMR Longitudinal Relaxation Properties of Water-Saturated Sandstones," *SPE Form. Eval.*, **3**, 622 (1988).

Mandava, S. S., A. T. Watson, and C. M. Edwards, "NMR Imaging of Saturation during Immiscible Displacements," *AIChE J.*, **36**, 1680 (1990).

Mansfield, P., and P. G. Morris, *NMR Imaging in Biomedicine*, Academic Press, San Francisco (1982).

Osment, P. A., K. J. Packer, M. J. Taylor, J. J. Attard, T. A. Carpenter, L. D. Hall, N. J. Herrod, and S. J. Doran, "NMR Imaging of Fluids in Porous Solids," *Phil. Trans. R. Soc. Lond.*, **A333**, 441 (1990).

Schmidt, E. J., K. K. Velasco, and A. M. Nur, "Quantifying Solid-Fluid Interfacial Phenomena in Porous Rocks with Proton Nuclear Magnetic Resonance," *J. Appl. Phys.*, **59**, 2788 (1986).

Timur, A., "Pulsed Nuclear Magnetic Resonance Studies of Porosity, Movable Fluids, and Permeability of Sandstone," *J. Pet. Tech.*, **21**, 775 (1969).

Watson, A. T., S. Chen, K. Kim, and G. Mejia, Subtask 2 of DOE Annual Report No. DE-FG07-89BC14446 (1991).

Manuscript received Aug. 3, 1992, and revision received Nov. 13, 1992.